Hydrodynamic simulations of oscillating shock waves in a sub-Keplerian accretion flow around black holes

Kinsuk Giri,[1] Sandip K. Chakrabarti,[1,2]★ Madan M. Samanta[2] and D. Ryu[3]

[1]*S. N. Bose National Centre for Basic Sciences, Salt Lake, Kolkata 700098, India*
[2]*Indian Centre for Space Physics, Chalantika 43, Garia Station Rd., Kolkata, 700084, India*
[3]*Department of Astron. Sp. Science, Chungnam Natl. Univ., Daejeon 305-764, South Korea*

ABSTRACT

We study the accretion processes on a black hole by a numerical simulation. We use a grid-based finite difference code for this purpose. We scan the parameter space spanned by the specific energy and the angular momentum and compare the time-dependent solutions with those obtained from theoretical considerations. We found several important results. (a) The time-dependent flow behaves close to a constant height model flow in the pre-shock region and a flow with vertical equilibrium in the post-shock region. (c) The infall time-scale in the post-shock region is several times higher than the free-fall time-scale. (b) There are two discontinuities in the flow, one being just outside of the inner sonic point. Turbulence plays a major role in determining the locations of these discontinuities. (d) The two discontinuities oscillate with two different frequencies and behave as a coupled harmonic oscillator. A Fourier analysis of the variation of the outer shock location indicates higher power at the lower frequency and lower power at the higher frequency. The opposite is true when the analysis of the inner shock is made. These behaviours will have implications in the spectral and timing properties of black hole candidates.

Key words: accretion, accretion discs – hydrodynamics – instabilities – shock waves.

1 INTRODUCTION

Understanding hydrodynamic behaviour of matter in the immediate vicinity of a black hole is extremely important as the emitted radiation intensity from the flow depends on the density and temperature at each flow element at each moment of time. Thus, the spectral and temporal properties of emitted radiation are directly determined by the hydrodynamic variables. Early known simulations were carried out by Hawley, Smarr & Wilson (1984a,b). However, the code may have been executed with flow parameters not giving rise to the steady shocks and as a result, the shocks were found to be propagating outward (but see, Hawley & Smarr 1986 where solutions with shock wave have been presented). Chakrabarti & Molteni (1993) and Molteni, Lanzafame & Chakrabarti (1994) used smoothed particle hydrodynamics (which preserves the specific angular momentum accurately because the 'particles' are toroidal in shape) to simulate one and two-dimensional sub-Keplerian flows and showed that flows become transonic and also produce standing shocks where they are predicted by well established theory of transonic flows (Chakrabarti 1990, hereafter C90). Formation of steady shocks was seen in simulations which uses a grid based

(Total Variation Diminishing or TVD) scheme also (Molteni, Ryu & Chakrabarti 1996a). Of course, if the initial condition of the flow is chosen to be random, the flow may show time-dependent behaviour as the steady transonic solution is possible only when the initial parameters are from a definite region of the parameter space. This was shown to be the case by Ryu et al. (1995) and Ryu, Chakrabarti & Molteni (1997). Using the TVD code, the latter authors showed that if the Rankine–Hugoniot condition is not satisfied, the shock is likely to oscillate. The oscillating shocks were also observed in presence of cooling (Molteni et al. 1996b; Chakrabarti, Acharyya & Molteni 2004) and were widely assumed to be the cause of the quasi-periodic oscillations (QPOs) observed in radiations emitted by accretion flows around black holes. Since the generic physical processes which cause the oscillations of the shocks, and therefore, the oscillations in the emitted radiation are the same in both the stellar and the massive/super-massive black holes, a thorough study of the nature of shock oscillations and the dependence of the oscillation frequencies on flow parameters is essential.

In this paper, we present the results of a series of simulations which basically sample the entire region of the parameter space spanned by the specific energy and specific angular momentum (Chakrabarti 1989, hereafter C89; C90), i.e. the parameter space relevant for non-dissipative, non-magnetic and axisymmetric

★E-mail: chakraba@bose.res.in

hydrodynamic accretion flows. We use an axisymmetric grid based TVD code for this purpose. We obtain a large number of very important results, which, to our knowledge, have never been published before. (a) Though as per injection condition at the outer boundary, the pre-shock flow properties match with the theoretical results of a constant height (CH) inflow, to our surprise, the post-shock flow properties match closely with the theoretical results obtained assuming a hybrid-model inflow (C89). What this means is that shock locations from simulations may be somewhat different from those of the theoretical results which assume either the CH or vertical equilibrium (VE) condition in the both sides of the shock. (b) The average infall time-scale from the post-shock region appears to be a few times longer than the free-fall time-scale due to turbulence. (c) For the majority of flow parameters, the shocks are found to be stable, though they may oscillate around a mean location. (d) Because of the strong turbulence close to a black hole which is formed due to the interaction of the incoming wave and the flow bounced back from the centrifugal barrier, a weak shock is formed closer to the black hole, though, both the normal outer shock and the inner shock seem to oscillate with the same frequencies – the outer shock shows more power at lower oscillation frequency and the inner shock shows more power at higher oscillation frequencies.

The plan of our paper is the following: in the next Section, we present the procedure of the TVD method. This is similar to what is used in Ryu et al. (1997) paper. In Section 3, we test the code with a simple zero angular momentum solution. In Molteni et al. (1996a), some test results with shock solutions were already presented. Present we discuss results of a large number of simulations and compare the results. Finally, in Section 4, we make concluding remarks.

2 METHODOLOGY OF THE NUMERICAL SIMULATIONS

The setup of our simulation is the same as in Ryu et al. (1997). We consider the adiabatic hydrodynamics of axisymmetric flows of gas under the Newtonian gravitational field of a point mass M_{bh} located at the centre in cylindrical coordinates $[R, \theta, Z]$. We also assume that the gravitational field of the black hole can be described by Paczyński & Wiita (1980),

$$\phi(R, Z) = -\frac{GM_{bh}}{r - r_g}, \tag{1}$$

where, $r = \sqrt{R^2 + Z^2}$ and the Schwarzschild radius is given by $r_g = 2GM_{bh}/c^2$. The black hole mass M_{bh}, the speed of light c, and the Schwarzschild radius r_g are assumed to be the units of the mass, the velocity and the length, respectively. We use $x = R/r_g$, and $z = Z/r_g$ as the dimensionless distances along x- and z-axis in the rest of the paper. We also assume a polytropic equation of state for the accreting (or outflowing) matter, $P = K\rho^\gamma$, where, P and ρ are the isotropic pressure and the matter density, respectively, γ is the adiabatic index (assumed in this paper to be constant throughout the flow, and is related to the polytropic index n by $\gamma = 1 + 1/n$) and K is related to the specific entropy of the flow. Since we ignore dissipation, the specific angular momentum $\lambda \equiv xv_\theta$ is constant everywhere. In C89 and C90, the steady solutions were classified according to the conserved flow parameters: the specific energy $\mathcal{E}$ and the specific angular momentum λ. At the outer boundary, where matter in injected, the velocity v_x is supplied and the sound speed a is computed from $\mathcal{E}$ from the dimensionless conserved

energy,

$$\mathcal{E} = \frac{v_x^2}{2} + \frac{a^2}{\gamma - 1} + \frac{\lambda^2}{2x^2} + g(x). \tag{2}$$

From equation (2), $g(x) = -1/2(x-1)^{-1}$. We assume a fixed Mach number $M = v_x/a = 10$ at the outer boundary and $z_o/x_o = 0.1$, where, z_o and x_o are the height and the radial distance of the injected matter at the outer boundary.

The numerical simulation code is grid based using the TVD scheme, originally developed by Harten (1983). It is an explicit, second-order accurate scheme which is designed to solve a hyperbolic system of the conservation equations, like the system of the hydrodynamic conservation equations. It is a non-linear scheme obtained by first modifying the flux function and then applying a non-oscillatory first-order accurate scheme to get a resulting second-order accuracy. In this way, we achieve the high resolution of a second-order accuracy while preserving the robustness of a non-oscillatory first-order scheme. The details of the code development are already in Ryu et al. (1995, 1997) and are not presented here.

The calculations have been done in a setting similar to that used in Ryu et al. (1997). The computational box occupies one quadrant of the $x - z$ plane with $0 \le x \le 50$ and $0 \le z \le 50$. We mimic the horizon ($x = 1$) by placing an absorbing boundary at a sphere of radius 1.5 inside which all the material is completely absorbed. To begin the simulation, we fill in the black hole surroundings with a very tenuous plasma of density $\rho_{bg} = 10^{-6}$ and the temperature as that of the incoming material. The incoming gas of density $\rho_{in} = 1$ enters the box through the outer boundary located at $x_o = 50$. The adiabatic index $\gamma = 4/3$ is chosen. In the absence of self-gravity and cooling, the density is scaled out, and thus the simulation results remain valid for accretion rate. At the outer boundary, $x_o = 50$ and thus $z_o = 5$. All the calculations have been done with 256×256 cells. Thus, each grid size is $\Delta x = \Delta z = 0.195$.

All the simulations are carried out assuming a stellar mass black hole ($M = 10\,M_\odot$). The results remain equally valid for massive/super-massive black holes, only the time and the length are to be scaled with the central mass. We carry out the simulations till several thousands of dynamical time-scales are passed. In reality, this corresponds to a few seconds in physical units.

3 SIMULATION RESULTS

In Molteni et al. (1996a), we presented the simulation results where the steady state solutions from the theoretical and the numerical methods were compared. Generally, the solutions were reproduced quite well and we do not repeat the tests any more.

First, we run a model where the injected matter has no specific angular momentum $\lambda = 0$ and follow the evolution. We compare the numerical solution with three models (Fig. 1), which are respectively the flow with a CH, the flow with an wedge shaped cross-section [constant angle (CA)] and the flow which is in VE (see Chakrabarti & Das 2001 for the definitions of these models). Here, the specific energy is chosen to be $\mathcal{E} = 0.023$. The flow approaches the black hole very smoothly and supersonically. We find that the numerical solution on the equatorial plane agrees very well with the theoretical results obtained with a CH flow but not with the other two model solutions.

In the next set of simulations, we include angular momentum. In Fig. 2, we present the classification of the solutions in the parameter space spanned by the conserved energy and angular momentum (C89, C90). In each region, the solution is qualitatively different.
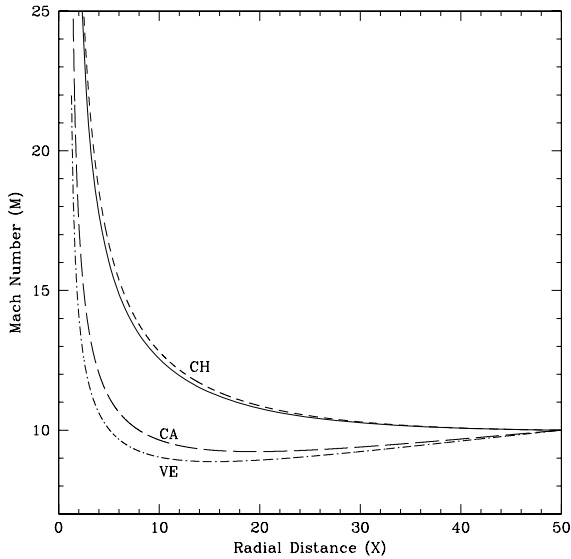
Figure 1. The variation of the Mach number of a $\lambda = 0.0$, $e = 0.023$ flow as a function of the radial distance from the black hole. The solid curve is the solution obtained from the simulation, while the other curves are the theoretical results for CH, CA and VE model. The time-dependent solution agrees well with that of a CH model flow.
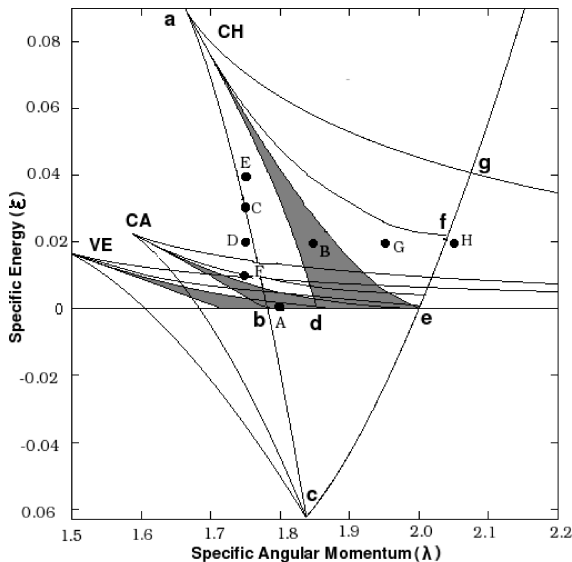
The classifications are made in all the three models, CH, CA and VE. For the detailed meaning of various divisions in the parameter space, see Chakrabarti (1996). Briefly, for CH model, the curve *abc* denotes the boundary between one (saddle type, on the left-hand side of the curve) and two sonic points (one saddle type and one circle type) in the flow solution. The region *abd* contains flow parameters which produce two saddle type and one circle type sonic points, but no steady shock condition is satisfied. The region *dae* has the same flow topologies as in *abd* but the steady shocks can form in accretion flows. The flow with parameters from *eaf* can form steady shocks only in winds and outflows. The solution topology in the region *fag* is same as that in *eaf*, but the steady shock condition is not satisfied. The points above *ag* have only one saddle-type sonic point. The solutions from points in *bcedb* have one saddle-type and one circle-type sonic points, however, the solutions do not extend to infinity. Flows with parameters from other regions do not have any kind of steady solution. Similar curves for the other two models, namely, CA and VE have similar meanings. We have shaded one region which produces standing shocks in each model. The cases (A)–(H) which have been run are given in Table 1 where the values
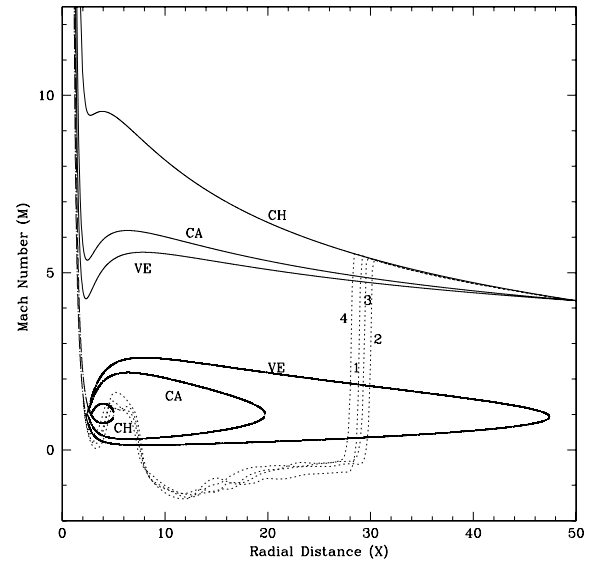

Figure 2. The parameter pairs $(\mathcal{E}, \lambda)$ marked by the filled circles on the classification diagram are used for numerical simulations (Cases A–H) in this paper. See text for details.

Figure 3. A comparison of the theoretical results obtained from the various models (marked) with those from the numerical simulations (dotted) for the same outer boundary condition (Case A). The solid curves are for the branch passing through the outer sonic point, and the long-dashed curves are for the branch passing through the inner sonic point. The Mach number variation on the equatorial plane is shown. The pre-shock region matches with that of a CH flow, while the post-shock region is similar to the flow in VE. The presence of two shocks in the numerical solution may be noted.

Table 1. The sonic points and shock locations (if any) obtained from three models for all the model runs presented in this paper.

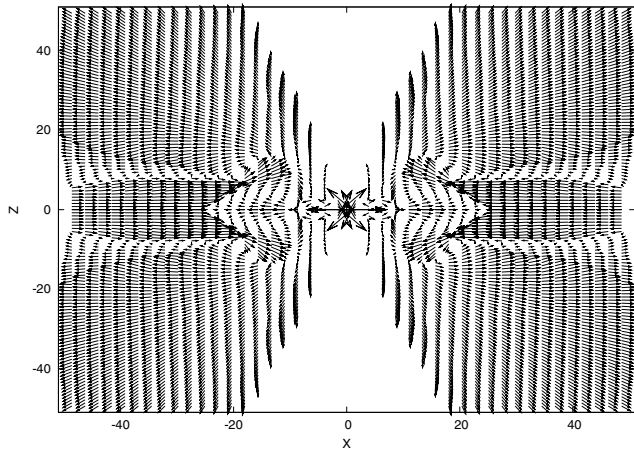| Case	$\mathcal{E}$	λ	VE x_{in}	x_{out}	x_s	Wedge shaped x_{in}	x_{out}	x_s	CH x_{in}	x_{out}	x_s
A	2.962e-04	1.80	2.321	1003.44	31.027	2.45	12.59	11.104	2.75	42.12	–
B	0.02	1.85	2.154	–	–	2.24	–	–	2.36	56.1	11.42
C	0.03	1.75	2.296	–	–	2.482	–	–	3.37	36.1	–
D	0.02	1.75	2.341	–	–	2.53	–	–	–	57.162	–
E	0.04	1.75	2.257	–	–	2.44	–	–	3.03	25.34	–
F	0.01	1.75	2.393	–	–	2.60	28.825	–	–	119.87	–
G	0.02	1.95	2.021	–	–	2.05	–	–	2.10	–	–
H	0.02	2.05	–	–	–	2.06	–	–	–	–	–

Figure 4. The velocity vectors of matter obtained from the simulation for Case A. Due to centrifugal barrier, matter bounces backward and forms the shock. The injected flow in the post-shock region is deflected away from the equatorial region and enters into the black hole supersonically from the higher elevation.

of the conserved energy and angular momentum $(\mathcal{E}, \lambda)$ are shown. These values are also marked inside Fig. 2 with filled circles to show that depending on the theoretical model, the same pair of flow parameters may or may not produce standing shocks. Our goal is to find out which model is vindicated by the numerical simulation results. In Table 1, we also present the locations of the inner and outer sonic points, if any, and the stable shock locations, if any.
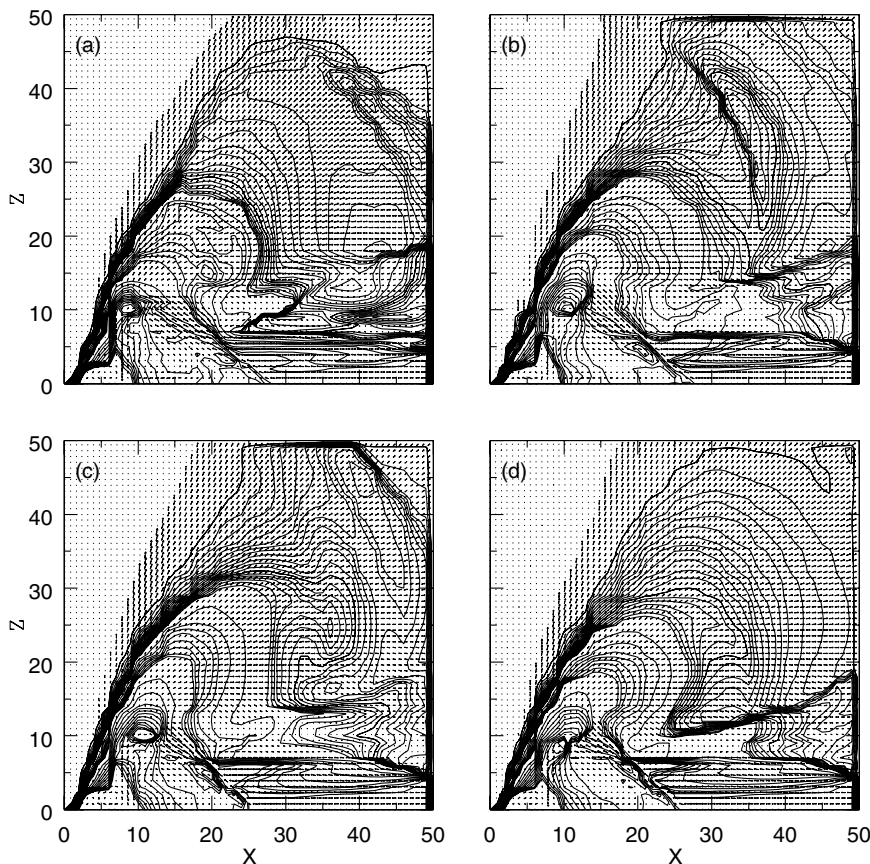

Figure 6. Variation of the shock locations in dimensionless units with time (seconds). Case A parameters are chosen for the simulation. A stellar mass $M = 10\,M_{\odot}$ black hole was chosen for the purpose of time computation. The time will scale with the mass of the black hole in this case since the dissipation of the flow and the radiative transfer were neglected.

In Fig. 3, we show the results of Case A. The parameters used are $\lambda = 1.80, \mathcal{E} = 2.962 \times 10^{-4}$. The dotted curves give the variation of the Mach number obtained from the numerical simulation (for the grid on the equatorial plane) at four consecutive times 1.90, 1.91,

Figure 5. Time-dependent behaviour is best seen in the density contours and velocity vector fields plotted at a regular time intervals. Time in seconds is marked on each box. The flow is deflected at the shock contributing to jets and outflows. Both the shock locations could be seen.
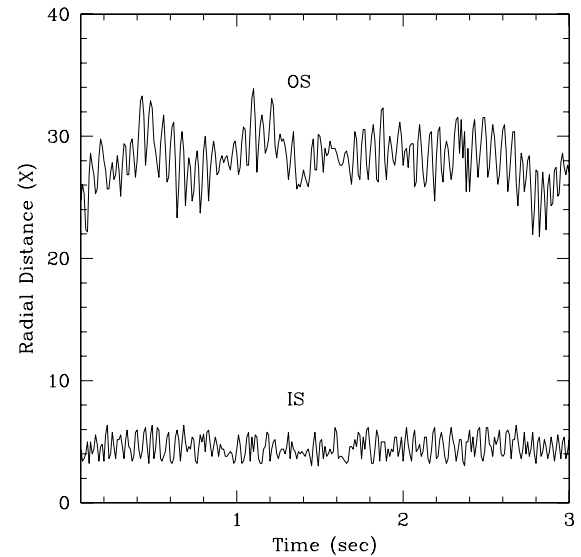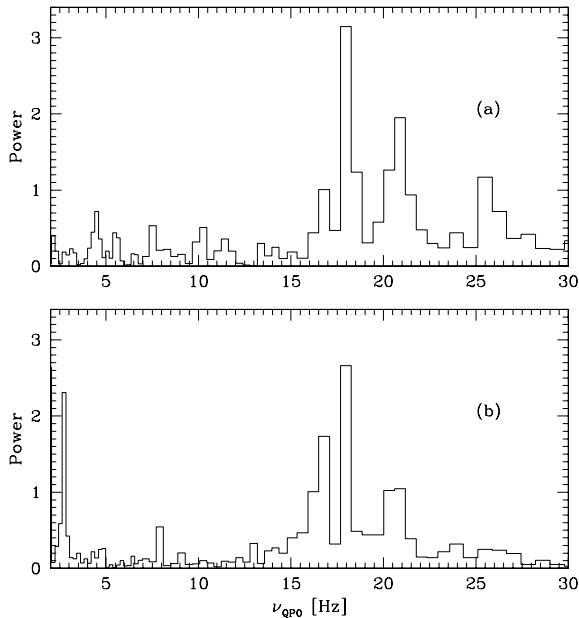
Figure 7. (a)–(b): Power density spectra of the time variation of the (a) inner and the (b) outer shock locations. The frequencies are calculated assuming $M = 10\,\mathrm{M}_{\odot}$. It will scale inversely with the mass of the black hole. The outer shock shows strong peaks at 1.56 and 17.97 Hz, while the inner shock peaks at 17.97 Hz only. Such an oscillation is thought to cause the periodic modulations in X-ray intensities from black hole candidates.
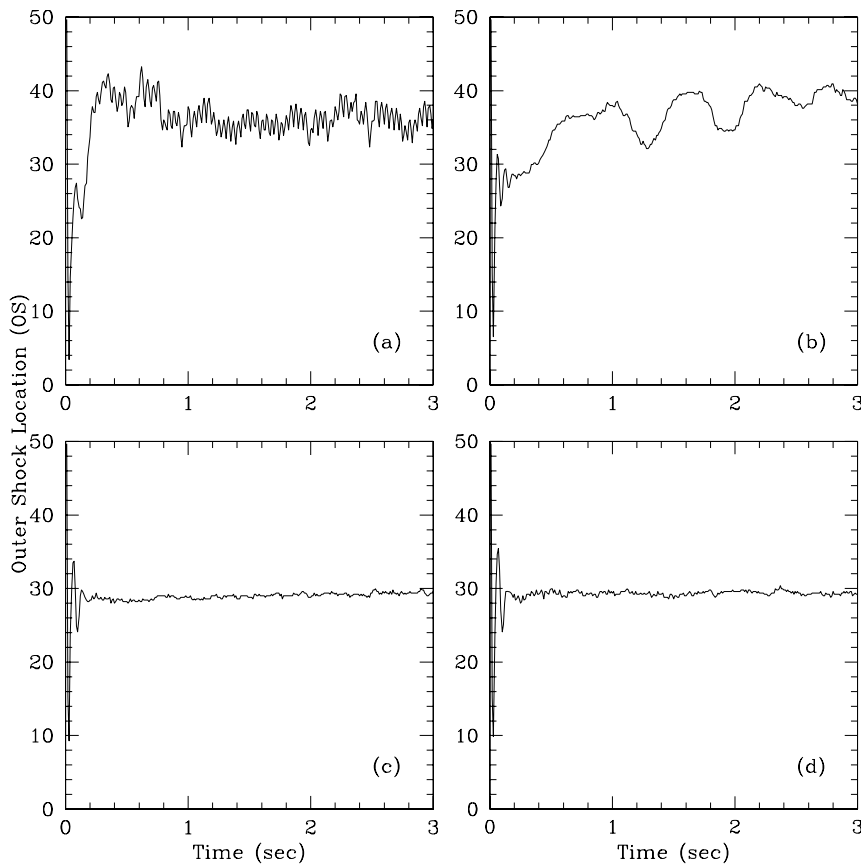
1.92 and 1.93 s. They are marked as 1–4, respectively. Superposed on these curves are the theoretically obtained solutions for various models (marked) with the same outer boundary condition – the solid curves are for supersonic branch and the long-dash-dotted curves are for subsonic branch. Theoretically, the steady shock is supposed to form at 31.027 in VE model (Table 1). Numerically, however, we find that the flow has formed a shock, but it is oscillating around a mean location. The flow Mach number jumps and becomes subsonic at around ($x \sim 28$). However, the shock location oscillates. In some part in the post-shock region, the flow has a 'negative' Mach number. In this case, the matter actually flows outward, bouncing back from the centrifugal barrier on the equatorial plane. At around $x \sim 7$, the flow becomes supersonic and again forms a relatively weaker 'inner shock' at around $x \sim 5$. This inner shock also oscillates.

Several important facts arise out of this exercise: (a) The inject matter behaves like a flow of constant thickness in the pre-shock region; (b) the Mach number variation in the post-shock region is closer to that of the flow in VE. Of course, the back-flow due to the centrifugal barrier is a major factor to influence the post-shock region. This is clearly seen in Fig. 4 where the velocity vectors have been plotted. The back-flow diverts the matter from the post-shock region to regions away from the equatorial plane and produces jets and outflows. Some of these diverted matters enter into the black hole from a height and become supersonic at around 2.5.

The behaviour of the time-dependent solution is evident in Figs 5(a)–(d) where we plot the velocity vector field and the density contours at regular intervals at times $t = 1.50$, 2.0, 2.5 and 3.0 s. The density contours in the post-shock region resemble those of a thick
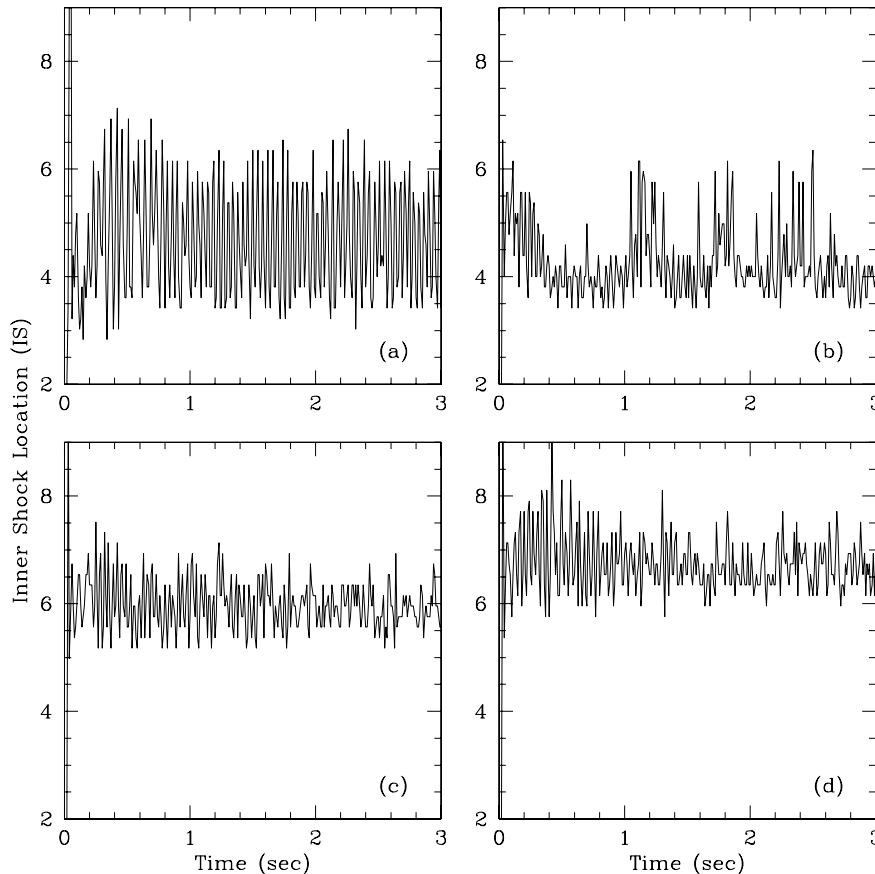

Figure 8. (a)–(d): Variation of the outer shock locations with time (seconds) when the angular momentum is increased: (a) $\lambda = 1.75$; (b) 1.85; (c) 1.95 and (d) 2.05. The oscillation frequencies are: (a) $\nu_{\mathrm{QPO}} = 2.54$ Hz and (b) 2.93, respectively. There are no oscillations in (c)–(d) due to dominance of turbulence.

Figure 9. (a)–(d): Variation of the inner shock locations with time (seconds) when the angular momentum is increased: (a) $\lambda = 1.75$; (b) 1.85; (c) 1.95 and (d) 2.05. The inner shock continues to oscillate in the entire range of angular momentum. The oscillation frequencies are (a) 24.70, (b) 25.50, (c) 28.61 and (d) 27.1 Hz, respectively.
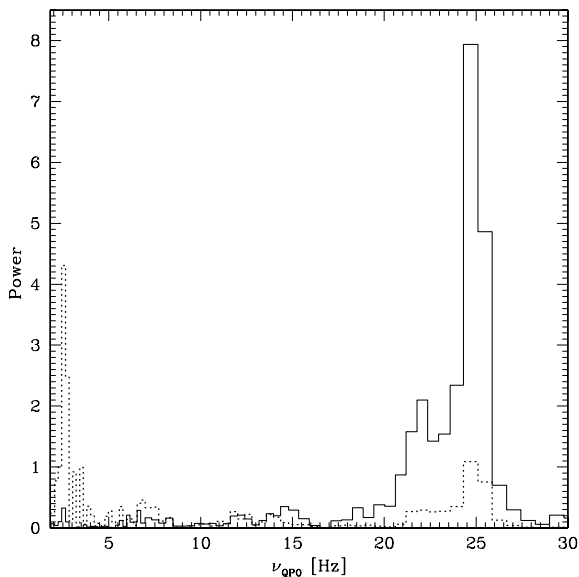

Figure 10. Power density spectra of the time variation of the inner (outer) shocks are shown by solid (dotted) histograms. Note that the PDS of the inner shock has more power at the higher frequency and that of the outer shock has more power at the lower frequency.

accretion disc (Paczyński & Wiita 1980), though our results are more realistic since the radial velocity is included here. The shock clearly moves around and the outflow also shows corresponding fluctuations. The density contours are for 0.01(0.01)0.1(0.1)1(1)13, where the density inside a parenthesis gives the interval and left and right numbers are 'from' and 'to' density values. The lowest density contour is at the highest altitude. The presence of two oscillating shocks is clear from successive figures. Some matter could be seen deflected outwards as outflows. The region close to Z-axis remains empty due to the centrifugal barrier. Turbulence slows down the flow and consequently, the infall time $t_{\text{inf}} = \Sigma \delta r / v_{\text{r}}$, where δr is the grid size and v_{r} is the local radial velocity, is longer than the free-fall time $t_{\text{ff}} = r^{3/2}$ in the post-shock region. A detailed computation using the radial velocity averaged over 20 grids in the vertical direction and using radial coordinate from the outer shock to the event horizon, shows that the ratio $R_t = t_{\text{inf}}/t_{\text{ff}}|_{\text{post−shock}} \sim 3.6$ in this case. In the pre-shock region $R_t \sim 1$.

We continue our detailed investigation of Case A. In Fig. 6, we show the variation of the outer and the inner shock locations (dimensionless unit) with time (in seconds). The oscillating nature settles down after an initial transient phase of $t \sim 0.06$. We clearly see the presence of oscillations in both the shocks, though the amplitudes are larger for the outer shock. The outer shock location oscillates between 26 and 32 and the inner shock oscillates between 3 and 5.

In Figs 7(a)–(b), we present the power density spectrum (PDS) of the time variation of the shock locations. In (a) and (b), the PDSs for
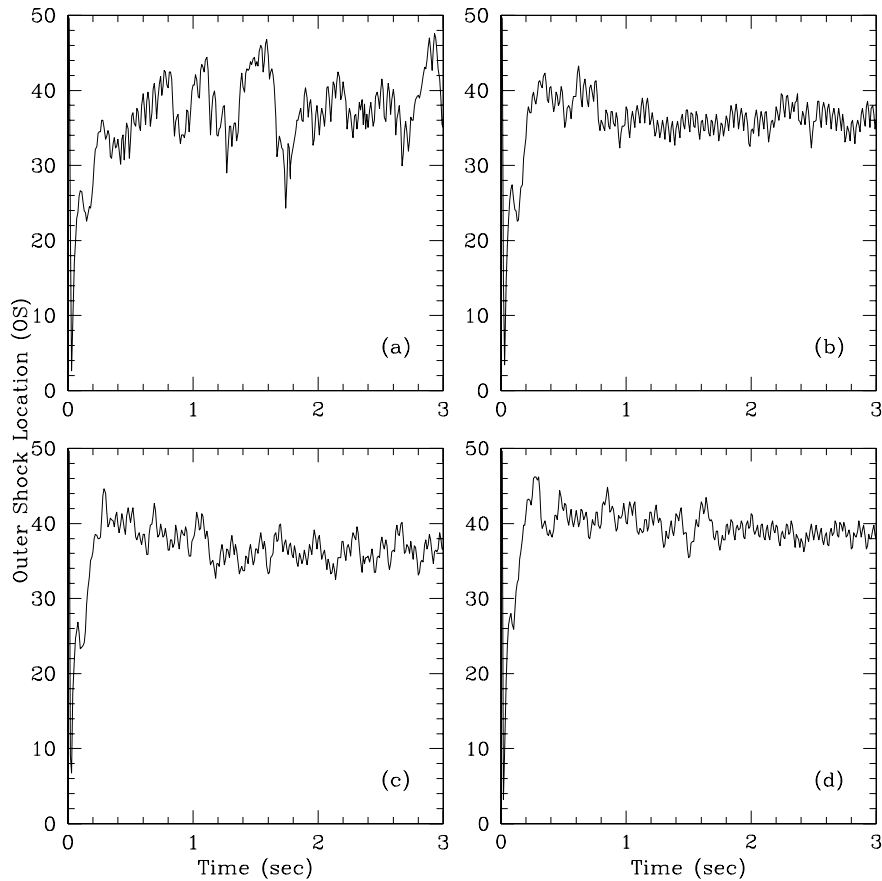
Figure 11. (a)–(d): Variation of the outer shock locations with time (seconds) when the specific energy is increased: (a) $\mathcal{E} = 0.01$; (b) 0.02; (c) 0.03 and (d) 0.04. The specific angular momentum remains the same at $\lambda = 1.75$. The oscillation frequencies are (a) $\nu_{QPO} = 22.6$, (b) 24.7, (c) 26.2 and (d)23.8, respectively.

the inner and the outer shock locations are shown. The outer shock shows a peak at 1.56 Hz, but otherwise, both the PDSs show strong peaks at ~18 Hz. In the subsonic flow of the post-shock region, the movement of the inner shock also perturbs the outer shock location and thus the high frequencies are the same. As will be discussed later, these oscillations can cause significant modulations of the X-ray intensity and cause the so-called QPOs in black hole candidates (Molteni et al. 1996b; Chakrabarti et al. 2004).

We now focus our attention to the oscillation properties of the shock locations by showing its dependence on the flow parameters. We choose the flow parameters of Cases D, B, G and H (Table 1 and Fig. 2). We only vary λ (1.75, 1.85, 1.95 and 2.05, respectively) while keeping the specific energy the same. In Figs 8(a)–(d), we compare the oscillations in the outer shock location and in Figs 9(a)–(d), we compare the oscillations in the inner shock location. The mean outer shock location slightly increases when λ increased from 1.75 to 1.85, but subsequently the shock becomes turbulent pressure dominated and not centrifugal pressure dominated, and the location does not change even with angular momentum. The mean inner shock location, on the contrary, shows a tendency to increase with angular momentum. The PDS gives the frequencies of oscillations to be $\nu_{QPO} = 2.54(24.70)$, $2.93(25.50)$, $-(28.61)$, $-(27.1)$ Hz for $\lambda = 1.75$, 1.85, 1.95 and 2.05 respectively for the outer (inner) shocks. The ratio R_t of the infall time and the free-fall time from the outer shock increases almost monotonically, which are 2.06, 3.06, 4.63 and 4.52 respectively. We also note that for low enough angular momentum, oscillations at the inner shock influences that at the outer shock. For higher angular momentum, however, the

perturbations are greatly washed out due to turbulence. As a result, only the inner shock oscillates and QPOs are produced at higher frequencies.

It is important to note that both the shocks are coupled together by the flow in between. As a result, both the shocks oscillate with higher and lower frequencies. The behaviour of the power density spectra is very interesting. In Fig. 10, we show the results of Case D, where both the PDSs are superimposed. The solid curve shows the PDS of the time variation of the inner shock location while the dotted curve shows the PDS of that of the outer shock. It seems that the inner shock has more power at the higher frequency peak, while the outer shock has more power at the lower frequency peak. Assuming that the hard X-rays are produced due to Compton scattering of soft X-rays by hot electrons in the post-shock region, this would mean that the hard X-rays will also modulate with high and low frequencies. The radiation from the post-(outer)shock region would participate in the QPOs in the lower frequency and the radiation from the relatively small post-(inner)shock region would participate in the high frequency oscillation.

We turn our attention to the behaviour of the oscillating shocks where the specific energy of the flow is changed while the specific angular momentum is kept fixed. The results we show are those of Cases (C)–(F) in Table 1. In Figs 11(a)–(d), we show the variation of the outer shock location and in Figs 12(a)–(d) we show the variation of the inner shock location. We assume $\lambda = 1.75$ and $\mathcal{E} = 0.01, 0.02, 0.03$ and 0.04 were used. Since the shocks are primarily centrifugal barrier supported, the locations of the shocks remain at similar distances, though, we see a small increase in the
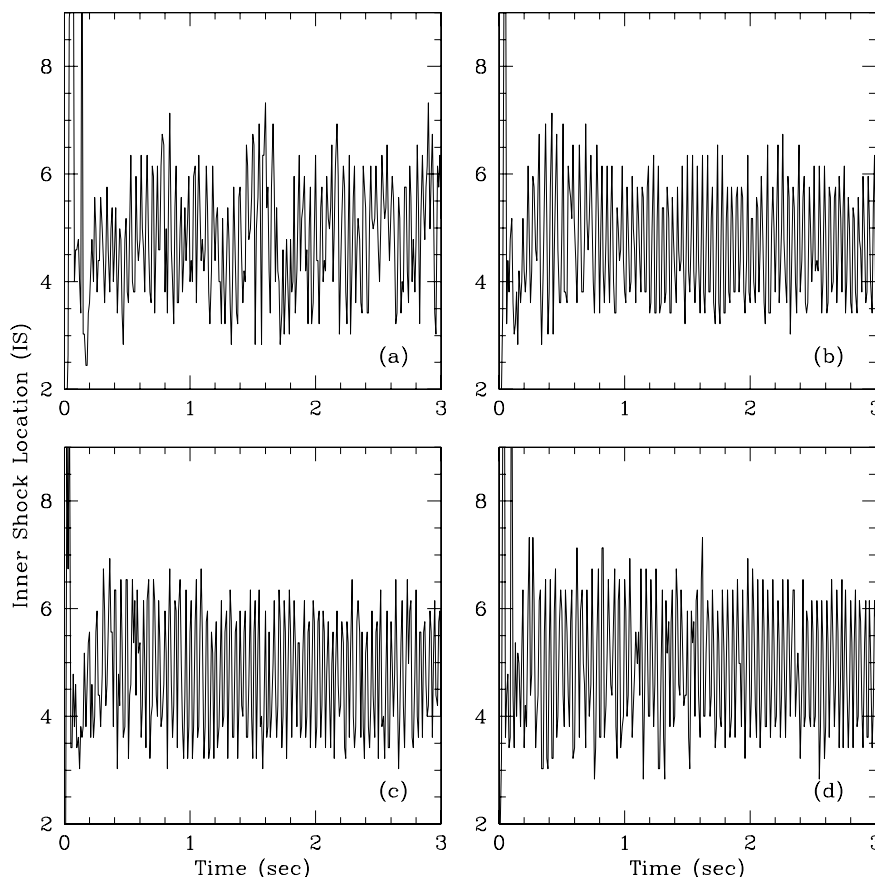
Figure 12. (a)–(d): Variation of the inner shock locations with time (seconds) when the specific energy is increased: (a) $\mathcal{E} = 0.01$; (b) 0.02; (c) 0.03 and (d) 0.04. The specific angular momentum remains the same at $\lambda = 1.75$. The oscillation frequencies are (a) $\nu_{QPO} = 2.4$, (b) 2.54, (c) 1.3 and (d)0.9, respectively.

mean shock (both the inner and the outer) locations with specific energy. This is expected from the theoretical point of view also. The frequency of oscillations of the outer (inner) shocks are 2.4 (22.6), 2.54(24.7), 1.3(26.2) and 0.9 (23.8), respectively. The ratio R_t of the infall time and free fall (averaged over 20 vertical grids above the equatorial plane) lies between 2 and 3.

We noted in Figs 4 and 5(a)–(d) that a considerable amount of matter is ejected outwards after they are bounced from the centrifugal barrier. It would be interesting to compute the amount of matter which leaves the grid system due to outflows. In Figs 13(a)–(b), we show the ratio of the outflow rate (calculated by adding those matter leaving the grid) and inflow rate (calculated from the outer boundary condition) for the four cases (Cases B, D, G and H) presented before. Here only λ is varied. For clarity, we present the results for $\lambda = 1.75$ and 1.85 in Fig. 13(a) and those for $\lambda = 1.95$ and 2.05 in Fig. 13(b). The mean ratios for the above cases are 0.42, 0.64, 0.56 and 0.58, respectively. We note that the amplitude and frequency of the fluctuations in the outflow rate are mainly dictated by the fluctuations of the outer shock location, though the inner shock modulates it further.

4 DISCUSSIONS AND CONCLUDING REMARKS

In this paper, we presented the results of two-dimensional hydrodynamic simulations of matter accreting on to a black hole. We systematically chose the flow parameters $(\mathcal{E}, \lambda)$ from the parameter space which provides complete set of solutions of a black hole ac-

cretion flow. The parameter space was classified into regions which may or may not produce standing shocks (C89, C90) in an inviscid flow. The classifications were made by using three different models of the flow, namely, a disc of constant thickness, a disc with conical wedge cross-section and a disc which is in VE (Chakrabarti & Das 2001). Our motivation was to study whether a simulated result behaves like a theoretical model throughout. We observed that the flow behaved like that of constant thickness before the shock. However, in the post-shock region, as the flow expands vertically due to higher thermal pressure, it behaved like that of a flow in VE. Secondly, the infall time in the post-shock region is several times larger as compared to the free-fall time, especially due to the formation of turbulence in the post-shock region. Thirdly, instead of only one possible shock transition, the flow shows the formation of two shocks, one very close to the black hole ($\sim$3–5) and the other farther away depending on the angular momentum. Both the shocks showed significant oscillations. While the inner shock oscillated faster than the outer shock, each of them also oscillated at the frequency of the other, though at a lesser power. These oscillations or their variants are long thought to cause the QPOs observed in black hole intensity (Molteni et al. 1996b; Chakrabarti et al. 2004). It is possible that not only the intermediate and low frequency QPOs are explained by this process, the high frequency QPOs may also be explained by the oscillations of the inner shock and the inner sonic point. However, since the volume of matter, participating in the inner shock oscillation is very small, the modulation at a high frequency would be negligible. We also observed that the outflows form from the post-shock region. The rates are specially high, and
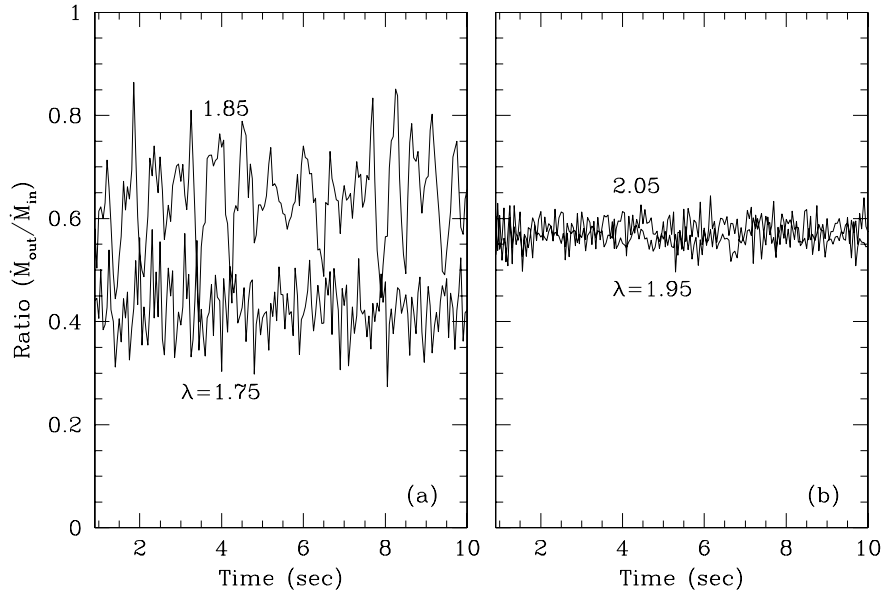
Figure 13. Variation of ratio of outflowing matter to injected matter with time when specific angular momentum is increased: (a) $\lambda = 1.75$, 1.85, (b) $\lambda = 1.95$, 2.05.

vary episodically. The amplitude and frequency of variation of the outflow rate is dictated by the amplitudes and frequencies of the two shocks. The outflow can be anywhere between 40 and 80 per cent of the inflow rate, provided the flow is sub-Keplerian. Since the Keplerian flows are subsonic, and therefore, strictly speaking no shocks, the outflows are not possible from a Keplerian disc in this model.

ACKNOWLEDGMENTS

REFERENCES

Chakrabarti S. K., 1989, ApJ, 347, 365 (C89)
Chakrabarti S. K., 1990, Theory of Transonic Astrophysical Flows. World Scientific, Singapore (C90)
Chakrabarti S. K., 1996, MNRAS, 283, 325
Chakrabarti S. K., Molteni D., 1993, ApJ, 417, 672
Chakrabarti S. K., Das S., 2001, MNRAS, 327, 808
Chakrabarti S. K., Acharyya K. A., Molteni D., 2004, A&A, 421
Harten A., 1983, J. Comp. Phys., 49, 357
Hawley J. F., Smarr L. L., 1986, in AIP Conf. Vol. 144, Magnetospheric Phenomena in Astrophysics, Am. Inst. Phys., New York, p. 263
Hawley J. F., Smarr L. L., Wilson J. R., 1984a, ApJ, 277, 296
Hawley J. F., Smarr L. L., Wilson J. R., 1984b, ApJ, 55, 211
Molteni D., Lanzafame G., Chakrabarti S. K., 1994, ApJ, 425, 161
Molteni D., Ryu D., Chakrabarti S. K., 1996a, ApJ, 470, 460
Molteni D., Sponholz H., Chakrabarti S. K., 1996b, ApJ, 457, 805
Paczyński B., Wiita P. J., 1980, 88, 23
Ryu D., Chakrabarti S. K., Molteni D., 1997, ApJ, 378, 388
Ryu D., Brown G. L., Ostriker J. P., Loeb A., 1995, ApJ, 452, 364

This paper has been typeset from a TeX/LaTeX file prepared by the author.